

Engineering entangled microwave photon states via multiphoton transitions between two cavities and a superconducting qubit

Yan-Jun Zhao,¹ Chang-Qing Wang,¹ Xiaobo Zhu,² and Yu-xi Liu^{1,3,*}

¹*Institute of Microelectronics, Tsinghua University, Beijing, 100084, China*

²*Institute of Physics, Chinese Academy of Sciences, Beijing, 100190, China*

³*Tsinghua National Laboratory for Information Science and Technology (TNList), Beijing 100084, China*

(Revised June 12, 2019)

It has been shown that there are not only transverse but also longitudinal couplings between microwave fields and a superconducting qubit with broken inversion symmetry of the potential energy. Using multiphoton processes induced by longitudinal coupling fields and frequency matching conditions, we design a universal algorithm to produce arbitrary superpositions of two-mode photon states of microwave fields in two separated transmission line resonators, which are coupled to a superconducting qubit. Based on our algorithm, we analyze the generation of evenly-populated states and NOON states. Compared to other proposals with only single-photon process, we provide an efficient way to produce entangled microwave states when the interactions between superconducting qubits and microwave fields are in the ultrastrong regime.

PACS numbers: 42.50.Dv, 42.50.Pq, 74.50.+r

I. INTRODUCTION

Superconducting transmission line resonators can be used as quantum data buses, quantum memories, single microwave photon detectors [1, 2]. They usually work in the microwave regime and can also be used as quantum nodes in so-called quantum networks [3, 4]. It is well known that the entanglement is one of the most important resources for quantum information processing [5], and microwave photons play a critical role in quantum state control for solid state quantum devices. Therefore, engineering arbitrarily entangled microwave photon states is a very fundamental issue for both solid state quantum information processing and quantum optics [6] on superconducting quantum chips.

Usually, nonclassical photon states of a single-mode cavity field are generated through the interaction between the cavity field and the two-level atom. The methods of generating nonclassical photon states can be classified into two ways. One is to engineer appropriate Hamiltonians in different evolution durations by tuning experimental parameters when the target state is being generated [7–10]. The other one is to obtain the target state via appropriately designed measurements [11]. The former one is deterministic, while the latter one is probabilistic and usually has a low probability to succeed. If the nonclassical state is generated using natural atomic systems, the latter method is usually more practical since most of parameters are not possible or not easy to be tuned. However, in artificial atomic systems, the former method is more appropriate because system parameters can be artificially controlled. For example, superconducting qubit circuits (SQCs) [12–19] provide us a very convenient way to deterministically engineer nonclassical states of a single-mode microwave field by varying the system parameters [7–10].

The method of deterministically generating entangled pho-

ton states using atomic systems can be tracked to that of generating entangled phonon states of two vibrational modes [20], in a trapped ion interacting with laser fields, by using different sideband transitions. However, the number of steps in such a method [20] exponentially depends on the maximum phonon numbers. A few proposals were put forward to overcome the exponential dependence of the phonon number by introducing auxiliary atomic energy levels [21, 22], using phonon number dependent interactions [23], or employing multiphonon transitions of high phonon numbers [22, 24]. These methods have successfully reduced the number of steps into quadratic polynomials of the maximum phonon numbers.

The generation of entangled microwave photon states of two modes using superconducting qubit has been studied [25–27], where a classically driven superconducting qubit with time-dependent frequency is coupled to two microwave fields in two separated cavities. The interaction Hamiltonian between the superconducting qubit and the cavity fields of two modes is described by the Jaynes-Cummings model. Therefore, there is only single photon transition in each step. However, the photon-number-dependent Stark effects [25–27] induced by the qubit-field coupling make it possible to independently implement operations for photon states. Thus, the number of steps also quadratically depends on the maximum photon number.

It has been shown that the superconducting qubit and the cavity field can have both transverse and longitudinal couplings when the inversion symmetry of the qubit potential energy is broken [28, 29]. The longitudinal coupling can induce multiphoton transitions [30] in different sidebands as in trapped ions [31, 32] and thus arbitrary photon states of a single-mode cavity field can be more conveniently engineered [30]. Motivated by studies [25–30], we study a method to generate entangled microwave photon states in two separated cavities coupled by a superconducting qubit using multiphoton transitions. We first show that the longitudinal couplings can induce two-mode multiphoton processes similar to those in trapped ions [33], and then study an efficient way to generate superposed two-mode photon states.

*Electronic address: yuxiliu@mail.tsinghua.edu.cn

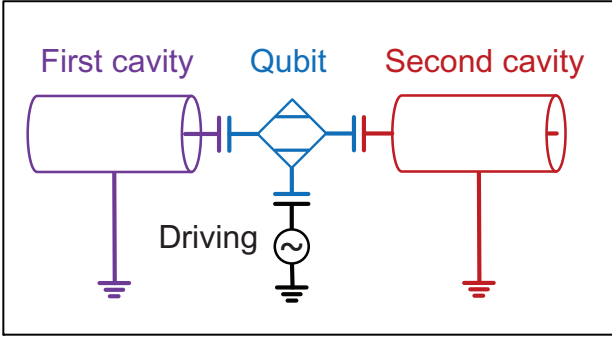


FIG. 1: (Color online) Schematic diagram for a driven qubit (in the middle with the blue color), which is coupled to two single-mode microwave fields of two separated cavities in the left with the purple color and the right with the red color, respectively. The first cavity field has the frequency ω_1 and the second one has the frequency ω_2 . The coupling strength is g_1 (g_2) between the qubit and the first (second) cavity field. The qubit is driven by a classical field (in the middle with the black color) with the frequency $\tilde{\omega}$ and Rabi frequency Ω .

The paper is organized as below. In Sec. II, an effective Hamiltonian, similar to that of trapped ions with two vibrational modes [33], is derived, and then different sideband transitions are discussed. In Sec. III, a new algorithm is introduced to generate arbitrary superpositions of two-mode photon states. In Sec. IV, we discuss how to choose parameters to obtain a high fidelity of the target state. In Sec. V, we numerically study the effects of both imperfect control pulses and the environment on the generated target state. In Sec. VI, the advantages and experimental feasibility are discussed. Finally, we summarize our results in Sec. VII.

II. THEORETICAL MODEL AND SIDEBAND EXCITATIONS

A. Basic Hamiltonian

As schematically shown in Fig. 1, we study a system where a superconducting qubit (SQ), i.e., a two level system, is coupled to two single-mode microwave fields in two separated cavities and driven by a classical field. The system Hamiltonian can be given by

$$\tilde{H} = \tilde{H}_q + H_r + \tilde{H}_g + \tilde{H}_d. \quad (1)$$

Here, \tilde{H}_q and H_r are the free Hamiltonians of the SQ and the cavity fields, respectively. Moreover, \tilde{H}_g is the interaction Hamiltonian between the SQ and cavity fields, and \tilde{H}_d is the interaction Hamiltonian between the SQ and the classical field. In the qubit basis, the qubit Hamiltonian is given by

$$\tilde{H}_q = \hbar\omega_q \frac{\tilde{\sigma}_z}{2}, \quad (2)$$

with $\tilde{\sigma}_x = |\tilde{g}\rangle\langle\tilde{e}| + |\tilde{e}\rangle\langle\tilde{g}|$ and $\tilde{\sigma}_z = |\tilde{e}\rangle\langle\tilde{e}| - |\tilde{g}\rangle\langle\tilde{g}|$. The parameter ω_q is the qubit frequency. The kets $|\tilde{g}\rangle$ and $|\tilde{e}\rangle$ denote the ground and excited states of the qubit, respectively.

The free Hamiltonian of two cavity fields is given by

$$H_r = \sum_{l=1}^2 \hbar\omega_l a_l^\dagger a_l, \quad (3)$$

where a_l (a_l^\dagger) is the annihilation (creation) operator of the l th cavity field with its frequency ω_l . The interaction Hamiltonian between the qubit and two cavity fields is

$$\tilde{H}_g = \sum_{l=1}^2 \hbar g_l (\tilde{\sigma}_z \cos \theta - \tilde{\sigma}_x \sin \theta) (a_l^\dagger + a_l), \quad (4)$$

where g_l is the coupling strength between the l th cavity field and the qubit, and θ is a parameter and depends on the inversion symmetry of the qubit potential energy.

Similarly, the interaction Hamiltonian between the qubit and classical field is given by

$$\tilde{H}_d = \hbar\Omega (\tilde{\sigma}_z \cos \theta - \tilde{\sigma}_x \sin \theta) \cos(\tilde{\omega}t + \phi), \quad (5)$$

where Ω is the coupling strength (or Rabi frequency) between the qubit and the driving field. The parameters $\tilde{\omega}$ and ϕ are the driving frequency and driving phase, respectively.

In Eqs. (4) and (5), when the qubit potential energy possesses inversion symmetry, i.e., $\cos \theta = 0$, there are only transverse couplings between the qubit and cavity fields [29]. If the rotating wave approximation is further made and there is no driving ($\Omega = 0$), Eq. (1) is reduced to extensively studied Jaynes-Cummings model [6]. When the qubit potential energy possesses a broken inversion symmetry [28, 29], i.e., $\cos \theta \neq 0$, there are both transverse and longitudinal couplings between the qubit and microwave fields. The broken inversion symmetry of the qubit potential energy can be achieved when the bias charge for the charge qubit or the bias flux for the flux qubit is tuned off the optimal point [28, 29]. But for the phase qubit, the inversion symmetry of the potential energy is always broken [34, 35]. Here, we will study a general method and not specify a particular qubit.

We now change the qubit basis into the current basis of the flux qubit or the charge basis of the charge qubit. This is equivalent to diagonalizing the operator $\tilde{\sigma}_z \cos \theta - \tilde{\sigma}_x \sin \theta$. In the new basis, the Hamiltonian in Eq. (1) becomes

$$H = H_q + H_r + H_g + H_d. \quad (6)$$

Here, the Hamiltonians H_q , H_g , and H_d are given by

$$H_q = \hbar\omega_x \frac{\sigma_x}{2} + \hbar\omega_z \frac{\sigma_z}{2}, \quad (7)$$

$$H_g = \sum_{l=1}^2 \hbar g_l \sigma_z (a_l^\dagger + a_l), \quad (8)$$

$$H_d = \hbar\Omega \sigma_z \cos(\tilde{\omega}t + \phi), \quad (9)$$

with $\sigma_x = |g\rangle\langle e| + |e\rangle\langle g|$, and $\sigma_z = |e\rangle\langle e| - |g\rangle\langle g|$. Hereafter, the parameters $\omega_x = \omega_q \sin \theta$ and $\omega_z = \omega_q \cos \theta$ are called transverse and longitudinal frequencies of the qubit, respectively. The kets $|g\rangle \equiv \tilde{R}_y(-\theta)|\tilde{g}\rangle$ and $|e\rangle \equiv \tilde{R}_y(-\theta)|\tilde{e}\rangle$ are persistent current states of the flux qubit or charge states of

the charge qubit. Here, $\tilde{R}_y(\varphi) = \exp(-i\varphi\tilde{\sigma}_y/2)$ is the rotation operator along the y -axis, with $\tilde{\sigma}_y = -i|\tilde{e}\rangle\langle\tilde{g}| + i|\tilde{g}\rangle\langle\tilde{e}|$. The parameter $\omega_z \neq 0$ results in longitudinal couplings between the qubit and microwave fields in Eq. (1). Below, we will show that $\omega_z \neq 0$ can induce two-mode multiphoton processes in the qubit, and then use these multiphoton processes to generate arbitrary superpositions of two-mode photon states.

B. Multiphoton processes and sideband excitations

To see how the multiphoton processes can be induced by the longitudinal coupling when $\omega_z \neq 0$, we now apply a unitary transformation

$$D = \exp \left[\sum_{l=1}^2 \eta_l \frac{\sigma_z}{2} (a_l^\dagger - a_l) \right], \quad (10)$$

to the Hamiltonian in Eq. (6). Then, we obtain an effective Hamiltonian

$$H_{\text{eff}} = DHD^\dagger = \hbar\omega_z \frac{\sigma_z}{2} + \hbar\Omega\sigma_z \cos(\tilde{\omega}t + \phi) + \sum_{l=1}^2 \hbar\omega_l a_l^\dagger a_l + \frac{\hbar\omega_x}{2} \left[\sigma_+ e^{\sum_{l=1}^2 \eta_l (a_l^\dagger - a_l)} + \text{H.c.} \right]. \quad (11)$$

It is clear that D is the displacement operator [6] of two-mode cavity fields. The displacement quantity is $\eta_l\sigma_z/2$ for the l th cavity field. Hereafter, we will call the picture after the operator D as the displacement picture. The ratios $\eta_l = 2g_l/\omega_l$ are called the Lamb-Dicke parameters in analogy to trapped ions [31, 32].

To understand the classical-field-assisted multiphoton transitions of two cavity fields in the qubit, we apply to Eq. (11) a time-dependent unitary transformation

$$U_d(t) = \exp \left[ix \frac{\sigma_z}{2} \sin(\tilde{\omega}t + \phi) \right], \quad (12)$$

with $x = 2\Omega/\tilde{\omega}$. Then, another effective Hamiltonian

$$H_{\text{eff}}^{(d)} = U_d H_{\text{eff}} U_d^\dagger - i\hbar U_d \frac{\partial}{\partial t} U_d^\dagger = \frac{\hbar}{2} \omega_z \sigma_z + \sum_{l=1}^2 \hbar\omega_l a_l^\dagger a_l + \frac{\hbar\omega_x}{2} \sum_{N=-\infty}^{\infty} [J_N \sigma_+ B_N(t) + \text{H.c.}], \quad (13)$$

can be derived, with the time-dependent term

$$B_N(t) = \exp \left[\sum_{l=1}^2 \eta_l (a_l^\dagger - a_l) + iN(\tilde{\omega}t + \phi) \right]. \quad (14)$$

Here, $J_N \equiv J_N(x)$ is the Bessel function of the first kind. Equation (13) shows that multiphoton transitions with different modes can be controlled by the classical field as in trapped ions [33].

In the interaction picture with the free Hamiltonian $H_0 = \sum_{l=1}^2 \hbar a_l^\dagger a_l + (\hbar\omega_z\sigma_z/2)$, Equation (13) becomes

$$H_{\text{int}} = \frac{\hbar\omega_x}{2} \sum_{N=-\infty}^{\infty} \sum_{\substack{m_1=0 \\ n_1=0}}^{\infty} \sum_{\substack{m_2=0 \\ n_2=0}}^{\infty} J_{Nm_1n_1}^{m_2n_2} a_1^{\dagger m_1} a_1^{n_1} a_2^{\dagger m_2} a_2^{n_2} \sigma_+ + \text{H.c.}, \quad (15)$$

where $J_{Nm_1n_1}^{m_2n_2} \equiv J_{Nm_1n_1}^{m_2n_2}(t)$ is the coupling strength between the qubit and cavity field with each different transition process, and its algebraic form is

$$J_{Nm_1n_1}^{m_2n_2} = \exp \left\{ i \left[N\tilde{\omega} + \omega_z + \sum_{l=1}^2 (m_l - n_l)\omega_l \right] t + iN\phi \right\} \times \exp \left(-\sum_l \frac{\eta_l^2}{2} \right) J_N(x) \frac{(-1)^{n_1+n_2} \eta_1^{m_1+n_1} \eta_2^{m_2+n_2}}{m_1!n_1!m_2!n_2!}. \quad (16)$$

Equation (15) describes the classical-field-assisted two-mode multiphoton processes as in trapped ions [33]. The magnitude of $J_{Nm_1n_1}^{m_2n_2}$ depends on ω_x , x , and η_l . We find

$$|J_{Nm_1n_1}^{m_2n_2}| = |J_N| \left| \frac{J_N^{m_1n_1}}{J_N} \right| \left| \frac{J_N^{m_2n_2}}{J_N} \right|, \quad (17)$$

where the properties of $J_N^{m_l n_l} \equiv J_N^{m_l n_l}(t)$ have been studied in Ref. [30]. The specific expression of $J_N^{m_l n_l}$ is given by

$$J_N^{m_l n_l} = \frac{(-1)^{n_l} J_N(x)}{m_l!n_l!} \eta_l^{m_l+n_l} \exp \left(-\frac{\eta_l^2}{2} \right) \times \exp \{i[N\tilde{\omega} + \omega_z + (m_l - n_l)\omega_l]t + iN\phi\}. \quad (18)$$

Similarly to Eq. (17), the magnitude of $J_N^{m_l n_l}$ can be rewritten as

$$|J_N^{m_l n_l}| = |J_N| \left| \frac{J_N^{m_l n_l}}{J_N} \right|. \quad (19)$$

It is clear that $|J_N^{m_l n_l}/J_N|$ is independent of the reduced driving strength x . From Eqs. (17)-(19), we know that both $|J_{Nm_1n_1}^{m_2n_2}|$ and $|J_N^{m_l n_l}|$ can be changed by adjusting x and η_l in a similar way. By introducing new variables $k_l = m_l - n_l$, we expand Eq. (15) in the Fock state basis, and then have

$$H_{\text{int}} = \hbar \sum_{Nn_1n_2} \sum_{\substack{k_1 \geq 0 \\ k_2 \geq 0}} W_{Nn_1n_2}^{k_1 k_2}(t) \sigma_+ \sigma_{n_1+|k_1|, n_1}^{(1)} \sigma_{n_2+|k_2|, n_2}^{(2)} + \hbar \sum_{Nn_1n_2} \sum_{\substack{k_1 \geq 0 \\ k_2 < 0}} W_{Nn_1n_2}^{k_1 k_2}(t) \sigma_+ \sigma_{n_1+|k_1|, n_1}^{(1)} \sigma_{n_2, n_2+|k_2|}^{(2)} + \hbar \sum_{Nn_1n_2} \sum_{\substack{k_1 < 0 \\ k_2 \geq 0}} W_{Nn_1n_2}^{k_1 k_2}(t) \sigma_+ \sigma_{n_1, n_1+|k_1|}^{(1)} \sigma_{n_2+|k_2|, n_2}^{(2)} + \hbar \sum_{Nn_1n_2} \sum_{\substack{k_1 < 0 \\ k_2 < 0}} W_{Nn_1n_2}^{k_1 k_2}(t) \sigma_+ \sigma_{n_1, n_1+|k_1|}^{(1)} \sigma_{n_2, n_2+|k_2|}^{(2)} + \text{H.c.} \quad (20)$$

Here, $\sigma_{n_l n'_l}^{(l)} = |n_l\rangle \langle n'_l|$ denotes the ladder operator of the l th cavity field. The time-dependent transition element $W_{Nn_1 n_2}^{k_1 k_2}(t)$ is given by

$$W_{Nn_1 n_2}^{k_1 k_2}(t) = \Omega_{Nn_1 n_2}^{k_1 k_2} \exp(i\Delta_N^{k_1 k_2} t), \quad (21)$$

where the complex transition amplitude $\Omega_{Nn_1 n_2}^{k_1 k_2}$ and detuning $\Delta_N^{k_1 k_2}$ are respectively

$$\Omega_{Nn_1 n_2}^{k_1 k_2} = \frac{\omega_x}{2} J_N(x) M_{n_1}^{k_1}(\eta_1) M_{n_2}^{k_2}(\eta_2) e^{iN\phi}, \quad (22)$$

$$\Delta_N^{k_1 k_2} = N\tilde{\omega} + \omega_z + k_1\omega_1 + k_2\omega_2. \quad (23)$$

The parameter $M_{n_l}^{k_l}$ is given by

$$M_{n_l}^{k_l}(\eta_l) = (-1)^{k_l \varepsilon_{k_l}} \frac{\eta_l^{|k_l|}}{e^{\eta_l^2/2}} \sqrt{\frac{n_l!}{(n_l + |k_l|)!}} L_{n_l}^{(|k_l|)}(\eta_l^2), \quad (24)$$

with

$$\varepsilon_k = \begin{cases} 1, & k < 0 \\ 0, & k \geq 0 \end{cases}, \quad (25)$$

$$L_n^{(k)}(x) = \sum_{l=0}^n \frac{(n+k)!}{(n-l)!} \frac{(-1)^l}{(l+k)!} \frac{x^l}{l!}. \quad (26)$$

Here, $L_n^{(k)}(x)$ is the generalized Laguerre polynomials. It is clear that the classical-field-assisted multiphoton transitions can be derived from Eq. (20) using different frequency-matching conditions.

C. Time evolution operators

We now give detailed discussions on how to engineer two-mode multiphoton processes by tuning the driving field. Let us assume that the driving field is tuned to satisfy the condition $\Delta_N^{k_1 k_2} = 0$. Then Eq. (20) can be reduced to an effective Hamiltonian $H_N^{k_1 k_2}$ when unwanted terms are neglected. Depending on the values of k_1 and k_2 , $H_N^{k_1 k_2}$ has different forms and is used to denote different sideband excitations. We will discuss the Hamiltonians $H_N^{k_1 k_2}$ and the corresponding evolution operators $U_N^{k_1 k_2}$ for different sideband transitions with different k_1 and k_2 .

(1) When $\Delta_N^{k_1 k_2} = 0$ with $k_1 \geq 0$ and $k_2 \geq 0$, from Eq. (23), we have $N < 0$, and therefore,

$$\omega_z + |k_1|\omega_1 + |k_2|\omega_2 = |N|\tilde{\omega}. \quad (27)$$

That is, when the qubit is the excited state and there are $|k_1|$ and $|k_2|$ photons inside the first and second cavity, then they can be converted into $|N|$ photons of the driving field, and vice versa. The Hamiltonian for this resonant condition is

$$H_N^{k_1 k_2} = \hbar \sum_{n_1=0}^{\infty} \sum_{n_2=0}^{\infty} \Omega_{Nn_1 n_2}^{k_1 k_2} \sigma_{+}^{(1)} \sigma_{n_1+|k_1|, n_1}^{(1)} \sigma_{n_2+|k_2|, n_2}^{(2)} + \text{H.c..} \quad (28)$$

The time evolution operator governed by the Hamiltonian in Eq. (28) is given by

$$\begin{aligned} U_N^{k_1 k_2} = & \sum_{n_1=0}^{\infty} \sum_{n_2=0}^{\infty} C_{Nn_1 n_2}^{k_1 k_2} \sigma_{gg} \sigma_{n_1 n_1}^{(1)} \sigma_{n_2 n_2}^{(2)} \\ & - \sum_{n_1=0}^{\infty} \sum_{n_2=0}^{\infty} i S_{Nn_1 n_2}^{k_1 k_2} \sigma_{+} \sigma_{n_1+|k_1|, n_1}^{(1)} \sigma_{n_2+|k_2|, n_2}^{(2)} \\ & - \sum_{n_1=0}^{\infty} \sum_{n_2=0}^{\infty} i S_{Nn_1 n_2}^{k_1 k_2*} \sigma_{-} \sigma_{n_1, n_1+|k_1|}^{(1)} \sigma_{n_2, n_2+|k_2|}^{(2)} \\ & + \sum_{n_1=0}^{\infty} \sum_{n_2=0}^{\infty} C_{Nn_1 n_2}^{k_1 k_2} \sigma_{ee} \sigma_{n_1+|k_1|, n_1+|k_1|}^{(1)} \sigma_{n_2+|k_2|, n_2+|k_2|}^{(2)} \\ & + \sum_{n_1=0}^{|k_1|-1} \sum_{n_2=0}^{|k_2|-1} \sigma_{ee} \sigma_{n_1 n_1}^{(1)} \sigma_{n_2 n_2}^{(2)}, \end{aligned} \quad (29)$$

where the parameters used in Eq. (29) are respectively

$$C_{Nn_1 n_2}^{k_1 k_2} \equiv C_{Nn_1 n_2}^{k_1 k_2}(t) = \cos\left(\left|\Omega_{Nn_1 n_2}^{k_1 k_2}\right|t\right), \quad (30)$$

$$S_{Nn_1 n_2}^{k_1 k_2} \equiv S_{Nn_1 n_2}^{k_1 k_2}(t) = e^{i\phi_{Nn_1 n_2}^{k_1 k_2}} \sin\left(\left|\Omega_{Nn_1 n_2}^{k_1 k_2}\right|t\right), \quad (31)$$

$$\phi_{Nn_1 n_2}^{k_1 k_2} = \arg\left(\Omega_{Nn_1 n_2}^{k_1 k_2}\right). \quad (32)$$

These notations will also be applied to the following discussions for other values of k_1 and k_2 .

(2) When $\Delta_N^{k_1 k_2} = 0$ with $k_1 \geq 0$ and $k_2 < 0$, from Eq. (23), we have

$$\pm |N|\tilde{\omega} + \omega_z + |k_1|\omega_1 = |k_2|\omega_2. \quad (33)$$

That is, when the qubit is the excited state and there are $|k_1|$ photons inside the first cavity, then they can be converted into $|k_2|$ photons of the second cavity by absorbing ($N \geq 0$) or emitting ($N < 0$) $|N|$ photons of the driving field, and vice versa. The Hamiltonian for this resonant condition is

$$\begin{aligned} H_N^{k_1 k_2} = & \hbar \sum_{n_1=0}^{\infty} \sum_{n_2=0}^{\infty} \Omega_{Nn_1 n_2}^{k_1 k_2} \sigma_{+} \sigma_{n_1+|k_1|, n_1}^{(1)} \sigma_{n_2, n_2+|k_2|}^{(2)} \\ & + \text{H.c..} \end{aligned} \quad (34)$$

The time evolution operator governed by the Hamiltonian in

Eq. (34) is given by

$$\begin{aligned}
U_N^{k_1 k_2} = & \sum_{n_1=0}^{\infty} \sum_{n_2=0}^{\infty} C_{N n_1 n_2}^{k_1 k_2} \sigma_{gg} \sigma_{n_1 n_1}^{(1)} \sigma_{n_2+|k_2|, n_2+|k_2|}^{(2)} \\
& - \sum_{n_1=0}^{\infty} \sum_{n_2=0}^{\infty} i S_{N n_1 n_2}^{k_1 k_2} \sigma_{+} \sigma_{n_1+|k_1|, n_1}^{(1)} \sigma_{n_2, n_2+|k_2|}^{(2)} \\
& - \sum_{n_1=0}^{\infty} \sum_{n_2=0}^{\infty} i S_{N n_1 n_2}^{k_1 k_2 *} \sigma_{-} \sigma_{n_1+|k_1|}^{(1)} \sigma_{n_2+|k_2|, n_2}^{(2)} \\
& + \sum_{n_1=0}^{\infty} \sum_{n_2=0}^{\infty} C_{N n_1 n_2}^{k_1 k_2} \sigma_{ee} \sigma_{n_1+|k_1|, n_1+|k_1|}^{(1)} \sigma_{n_2, n_2}^{(2)} \\
& + \sum_{n_1=0}^{\infty} \sum_{n_2=0}^{|k_2|-1} \sigma_{gg} \sigma_{n_1 n_1}^{(1)} \sigma_{n_2 n_2}^{(2)} \\
& + \sum_{n_1=0}^{|k_1|-1} \sum_{n_2=0}^{\infty} \sigma_{ee} \sigma_{n_1 n_1}^{(1)} \sigma_{n_2 n_2}^{(2)}. \tag{35}
\end{aligned}$$

(3) When $\Delta_N^{k_1 k_2} = 0$ with $k_1 < 0, k_2 \geq 0$, from Eq. (23), we have

$$\pm |N| \tilde{\omega} + \omega_z + |k_2| \omega_2 = |k_1| \omega_1. \tag{36}$$

That is, when the qubit is in the excited state and there are $|k_2|$ photons inside the second cavity, then they can be converted into $|k_1|$ photons of the first cavity by absorbing ($N \geq 0$) or emitting ($N < 0$) $|N|$ photons of the driving field, and vice versa. The Hamiltonian for this resonant condition is

$$\begin{aligned}
H_N^{k_1 k_2} = & \sum_{n_1=0}^{\infty} \sum_{n_2=0}^{\infty} \hbar \Omega_{N n_1 n_2}^{k_1 k_2} \sigma_{+} \sigma_{n_1, n_1+|k_1|}^{(1)} \sigma_{n_2+|k_2|, n_2}^{(2)} \\
& + \text{H.c.} \tag{37}
\end{aligned}$$

The time evolution operator governed by the Hamiltonian in Eq. (37) is given by

$$\begin{aligned}
U_N^{k_1 k_2} = & \sum_{n_1=0}^{\infty} \sum_{n_2=0}^{\infty} C_{N n_1 n_2}^{k_1 k_2} \sigma_{gg} \sigma_{n_1+|k_1|, n_1+|k_1|}^{(1)} \sigma_{n_2, n_2}^{(2)} \\
& - \sum_{n_1=0}^{\infty} \sum_{n_2=0}^{\infty} i S_{N n_1 n_2}^{k_1 k_2} \sigma_{+} \sigma_{n_1, n_1+|k_1|}^{(1)} \sigma_{n_2+|k_2|, n_2}^{(2)} \\
& - \sum_{n_1=0}^{\infty} \sum_{n_2=0}^{\infty} i S_{N n_1 n_2}^{k_1 k_2 *} \sigma_{-} \sigma_{n_1+|k_1|, n_1}^{(1)} \sigma_{n_2+|k_2|, n_2}^{(2)} \\
& + \sum_{n_1=0}^{\infty} \sum_{n_2=0}^{\infty} C_{N n_1 n_2}^{k_1 k_2} \sigma_{ee} \sigma_{n_1, n_1}^{(1)} \sigma_{n_2+|k_2|, n_2+|k_2|}^{(2)} \\
& + \sum_{n_1=0}^{|k_1|-1} \sum_{n_2=0}^{\infty} \sigma_{gg} \sigma_{n_1 n_1}^{(1)} \sigma_{n_2 n_2}^{(2)} \\
& + \sum_{n_1=0}^{\infty} \sum_{n_2=0}^{|k_2|-1} \sigma_{ee} \sigma_{n_1 n_1}^{(1)} \sigma_{n_2 n_2}^{(2)}. \tag{38}
\end{aligned}$$

(4) When $\Delta_N^{k_1 k_2} = 0$ with $k_1 < 0, k_2 < 0$, from Eq. (23), we have

$$\pm |N| \tilde{\omega} + \omega_z = |k_1| \omega_1 + |k_2| \omega_2. \tag{39}$$

This is, when the qubit is in the excited state, then it can emit $|k_1|$ photons of the first cavity mode and $|k_2|$ photons of the second cavity mode by absorbing ($N \geq 0$) or emitting ($N < 0$) $|N|$ photons of the driving field, and vice versa. The Hamiltonian for this resonant condition is

$$\begin{aligned}
H_N^{k_1 k_2} = & \sum_{n_1=0}^{\infty} \sum_{n_2=0}^{\infty} \hbar \Omega_{N n_1 n_2}^{k_1 k_2} \sigma_{+} \sigma_{n_1, n_1+|k_1|}^{(1)} \sigma_{n_2, n_2+|k_2|}^{(2)} \\
& + \text{H.c..} \tag{40}
\end{aligned}$$

The time evolution operator governed by the Hamiltonian in Eq. (40) is given by

$$\begin{aligned}
U_N^{k_1 k_2} = & \sum_{n_1=0}^{\infty} \sum_{n_2=0}^{\infty} C_{N n_1 n_2}^{k_1 k_2} \sigma_{gg} \sigma_{n_1+|k_1|, n_1+|k_1|}^{(1)} \sigma_{n_2+|k_2|, n_2+|k_2|}^{(2)} \\
& - \sum_{n_1=0}^{\infty} \sum_{n_2=0}^{\infty} i S_{N n_1 n_2}^{k_1 k_2} \sigma_{+} \sigma_{n_1, n_1+|k_1|}^{(1)} \sigma_{n_2, n_2+|k_2|}^{(2)} \\
& - \sum_{n_1=0}^{\infty} \sum_{n_2=0}^{\infty} i S_{N n_1 n_2}^{k_1 k_2 *} \sigma_{-} \sigma_{n_1+|k_1|, n_1}^{(1)} \sigma_{n_2+|k_2|, n_2}^{(2)} \\
& + \sum_{n_1=0}^{\infty} \sum_{n_2=0}^{\infty} C_{N n_1 n_2}^{k_1 k_2} \sigma_{ee} \sigma_{n_1, n_1}^{(1)} \sigma_{n_2, n_2}^{(2)} \\
& + \sum_{n_1=0}^{|k_1|-1} \sum_{n_2=0}^{|k_2|-1} \sigma_{gg} \sigma_{n_1 n_1}^{(1)} \sigma_{n_2 n_2}^{(2)}. \tag{41}
\end{aligned}$$

Because the Hamiltonian derived in Eq. (15) is similar to that of the trapped ions [24], the algorithm using two-mode multi-phonon processes in trapped ions can be directly applied into our model, and different superpositions of two-mode photons can be generated. As a special case, two-mode Fock states of high photon numbers can in principle be more efficiently generated with just two steps as single-mode Fock states of high photon numbers [30]. However, we here design a new algorithm via different sideband transitions of low photon numbers by tuning the driving field with properly selecting the parameters $\omega_z, \omega_x, \omega_l$, and η_l . The detailed discussions of parameter selection will be given in Sec. IV.

III. ALGORITHM FOR STATE GENERATION

Let us first study a universal algorithm for generating arbitrary two-mode microwave photon states using sideband transitions with the following four Hamiltonians $H_1^{1\bar{1}}, H_1^{\bar{1}0}, H_1^{0\bar{1}}$, and H_1^{00} . Here, for the compact of notations, we have used \bar{k} to represent $-k$ with $k > 0$. For instance, $H_1^{1\bar{1}}$ is actually $H_N^{k_1 k_2}$ with $N = -1, k_1 = 1$, and $k_2 = -1$. For different N, k_1 , and k_2 , the interaction Hamiltonian $H_N^{k_1 k_2}$ and its time evolution operator $U_N^{k_1 k_2}$ have already been given in Sec. II C. Below, we will first study how to generate the target state by choosing pulse durations, frequencies, and phases of the driving fields at each generation step with different sideband excitations, and then we will apply our algorithm to the generation of NOON states and discuss particular properties of the algorithm.

A. Universal algorithm for generating arbitrary two-mode microwave photon states

We note that the state generation in our algorithm is studied in the displacement picture with the unitary transformation as shown in Eq. (10). The arbitrary quantum states, we expect to be generated, is written as

$$|\psi_f\rangle = \sum_{n_1+n_2 \leq N_{\max}} C_{n_1, n_2} |n_1, n_2\rangle |g\rangle, \quad (42)$$

where $|n_1, n_2\rangle$ means that the first and second cavities contain n_1 and n_2 photons, respectively, and $|g\rangle$ means that the qubit is in the ground state. Besides, N_{\max} and C_{n_1, n_2} mean the maximum photon number and the probability amplitude on the state $|n_1, n_2\rangle |g\rangle$, respectively. We assume that the system is initially in the state

$$|\psi_0\rangle = |0, 0\rangle |g\rangle. \quad (43)$$

We suppose the target state $|\psi_f\rangle$ can be generated by alternately switching on and off the two-mode transitions $H_1^{1\bar{1}}$, $H_1^{\bar{1}0}$, $H_1^{0\bar{1}}$, and H_1^{00} . With the designed time evolution operators, the state generation procedure can be represented by,

$$\begin{aligned} |\psi_f\rangle &= \prod_{\nu=f}^1 \left[\bar{U}_\nu^\dagger(t_\nu) U_1^{p_\nu}(t_\nu) \bar{U}_\nu(0) \right] |\psi_0\rangle \\ &= \left[\bar{U}_f^\dagger(t_f) U_1^{p_f}(t_f) \bar{U}_f(0) \right] \cdots \\ &\quad \left[\bar{U}_1^\dagger(t_1) U_1^{p_1}(t_1) \bar{U}_1(0) \right] |0, 0\rangle |g\rangle, \end{aligned} \quad (44)$$

where $p_\nu \in \{1\bar{1}, \bar{1}0, 0\bar{1}, 00\}$ denotes the transition type for the ν th step, and t_ν is the time duration for the ν th step. The time evolution operator $\bar{U}_\nu(t_\nu)$ is given by

$$\begin{aligned} \bar{U}_\nu(t_\nu) &= \exp \left[i \left(\omega_z \frac{\sigma_z}{2} + \omega_1 a_1^\dagger a_1 + \omega_2 a_2^\dagger a_2 \right) t_\nu \right] \\ &\quad \times \exp \left[ix \frac{\sigma_z}{2} \sin(\tilde{\omega}_\nu t_\nu + \phi_\nu) \right]. \end{aligned} \quad (45)$$

As discussed in above, the transitions of different types can be achieved by changing the frequency $\tilde{\omega}$ of the driving field, which is denoted by $\tilde{\omega}_\nu$ for the ν th step. The phase of the driving field for the ν th step is denoted by ϕ_ν . We can express Eq. (44) in another equivalent form of iteration,

$$|\psi_{\nu-1}\rangle = \bar{U}_\nu^\dagger(0) U_1^{p_\nu\dagger}(t_\nu) \bar{U}_\nu(t_\nu) |\psi_\nu\rangle, \quad (46)$$

with $|\psi_0\rangle$ and $|\psi_f\rangle$ given in Eqs. (43) and (42), respectively. The ket $|\psi_\nu\rangle$ is the state after the ν th step. We note that the subscript f of $|\psi_f\rangle$ in Eq. (44) denotes the number of the final step. Equation (46) means that the initial state is restored from the target state by a composition of sideband transitions with proper time durations, frequencies and phases of driving fields. It is a recursion algorithm.

Without loss of generality, we use the maximum photon number $N_{\max} = 2$ as an example to show our algorithm. The more general case with arbitrary N_{\max} is given in Appendix A. The detailed steps for generating the target state

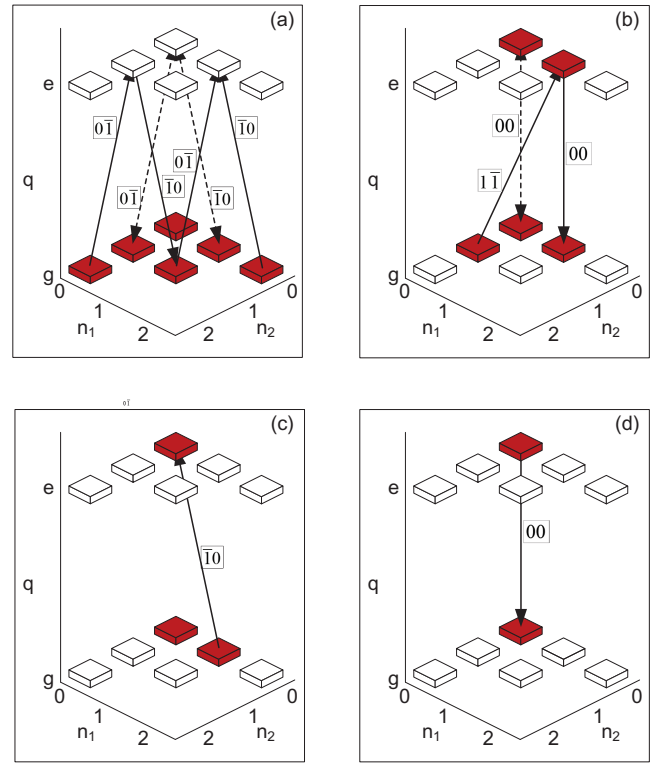


FIG. 2: (Color online) Universal algorithm for generating arbitrary two-mode superposition state. The n_1 and n_2 -axis respectively denote the photon number of the first and second mode. The two-mode photon state is denoted by $|n_1, n_2\rangle$. The qubit state is represented by the q -axis with $q = g$ or e respectively denoting the ground state $|g\rangle$ or excited state $|e\rangle$. The state component $|n_1, n_2\rangle |q\rangle$ is represented by a block at the location (n_1, n_2, q) . If a state component is occupied, we color the corresponding block with red; otherwise, the block is left uncolored. The arrows respectively represent the “ $\bar{1}0$ ”, “ $0\bar{1}$ ”, “ $1\bar{1}$ ”, and “ 00 ” transitions with transition types labeled aside them. The solid arrow indicates a population transfer from the starting state to the end state, while the dashed arrow indicates the inevitable irrelevant oscillation when the desired population transfer is implemented. (a) Schematic diagram for transferring the populations on states $|0, 2\rangle |g\rangle$, $|1, 1\rangle |g\rangle$, and $|2, 0\rangle |g\rangle$ to the state $|1, 0\rangle |e\rangle$. This is achieved by consecutively using “ $0\bar{1}$ ”, “ 10 ”, “ $0\bar{1}$ ”, and “ 10 ” transitions. (b) Schematic diagram for transferring populations on states $|0, 1\rangle |g\rangle$ and $|1, 0\rangle |e\rangle$ to the state $|1, 0\rangle |g\rangle$. This is achieved by consecutively using “ $1\bar{1}$ ” and “ 00 ” transitions. (c) Schematic diagram for transferring the population on the state $|1, 0\rangle |g\rangle$ to the state $|0, 0\rangle |e\rangle$. This is achieved by using a “ $\bar{1}0$ ” transition. (d) Schematic diagram for transferring the population on the state $|0, 0\rangle |e\rangle$ to the state $|0, 0\rangle |g\rangle$. This is achieved by using a “ 00 ” transition.

with $N_{\max} = 2$ using our recursion algorithm from the final state $|\psi_f\rangle$ are described as the following four procedures.

Procedure (i). As schematically shown in Fig. 2(a), from the final state $|\psi_f\rangle$, we first transfer the populations in the state space spanned by $\{|n_1, n_2\rangle |g\rangle\}$ with $n_1 + n_2 = 2$ to the state $|1, 0\rangle |e\rangle$. This procedure consists of four steps.

1. In the step f , the “ $0\bar{1}$ ” transition is switched on. Meanwhile, the pulse duration t_f and phase ϕ_f of the driving

field are properly chosen so that the population on the state $|0, 2\rangle|g\rangle$ is transferred to the state $|0, 1\rangle|e\rangle$. From Eq. (46), we thus obtain the state $|\psi_{f-1}\rangle$.

2. In the step $f - 1$, “ $\bar{1}0$ ” transition is switched on. Meanwhile, the pulse duration t_{f-1} and phase ϕ_{f-1} of the driving field are properly chosen so that the population on the state $|0, 1\rangle|e\rangle$ is transferred to the state $|1, 1\rangle|g\rangle$. We thus obtain the state $|\psi_{f-2}\rangle$.
3. In the step $f - 2$, “ $0\bar{1}$ ” transition is switched on. Meanwhile, the pulse duration t_{f-2} and phase ϕ_{f-2} of the driving field are properly chosen so that the population on the state $|1, 1\rangle|g\rangle$ is transferred to the state $|1, 0\rangle|e\rangle$. We thus obtain the state $|\psi_{f-3}\rangle$.
4. In the step $f - 3$, “ $\bar{1}0$ ” transition is switched on. Meanwhile, the pulse duration t_{f-3} and phase ϕ_{f-3} of the driving field are properly chosen so that the population on the state $|2, 0\rangle|g\rangle$ is transferred to the state $|1, 0\rangle|e\rangle$. We thus obtain the state $|\psi_{f-4}\rangle$.

Procedure (ii). As schematically shown in Fig. 2(b), starting from the state $|\psi_{f-4}\rangle$, we need to transfer the populations in the state space spanned by $\{|0, 1\rangle|g\rangle, |1, 0\rangle|e\rangle\}$ to the state $|1, 0\rangle|g\rangle$. This procedure consists of two steps.

1. In the step $f - 4$, “ $1\bar{1}$ ” transition is switched on. Meanwhile, the pulse duration t_{f-4} and phase ϕ_{f-4} of the driving field are properly chosen so that the population on the state $|0, 1\rangle|g\rangle$ is transferred to the state $|1, 0\rangle|e\rangle$. We thus obtain the state $|\psi_{f-5}\rangle$.
2. In the step $f - 5$, “ 00 ” transition is switched on. Meanwhile, the pulse duration t_{f-5} and phase ϕ_{f-5} of the driving field are properly chosen so that the population on the state $|1, 0\rangle|e\rangle$ is transferred to the state $|1, 0\rangle|g\rangle$. We thus obtain the state $|\psi_{f-6}\rangle$.

Procedure (iii). This procedure is similar to Procedure (i). As schematically shown in Fig. 2(c), starting from the state $|\psi_{f-6}\rangle$, here we need to transfer the population on the state $|1, 0\rangle|g\rangle$ to the state $|0, 0\rangle|e\rangle$. This procedure consists of only one step.

In the step $f - 6$, “ $\bar{1}0$ ” transition is switched on. Meanwhile, the pulse duration t_{f-6} and phase ϕ_{f-6} are properly chosen so that the population on the state $|1, 0\rangle|g\rangle$ is transferred to the state $|0, 0\rangle|e\rangle$. We thus obtain the state $|\psi_{f-7}\rangle$.

Procedure (iv). This procedure is similar to the Procedure (ii). As schematically shown in Fig. 2(d), starting from the state $|\psi_{f-7}\rangle$, we need to transfer the population on the state $|0, 0\rangle|e\rangle$ to the state $|0, 0\rangle|g\rangle$. This procedure only consists of one step.

In the step $f - 7$, “ 00 ” transition is switched on. Meanwhile, the pulse duration t_{f-7} and phase ϕ_{f-7} of the driving field are properly chosen so that the population on the state $|0, 0\rangle|e\rangle$ is transferred to the state $|0, 0\rangle|g\rangle$. We thus obtain the state $|\psi_{f-8}\rangle = |0, 0\rangle|g\rangle$.

Therefore, the target $|\psi_f\rangle$ can be generated from the initial state $|\psi_{f-8}\rangle$ using inverse processes from the Procedure (iv) to the Procedure (i). We note $|\psi_{f-8}\rangle \equiv |\psi_0\rangle = |0, 0\rangle|g\rangle$. Thus, we obtain the total step number $f = 8$ by setting $f - 8 = 0$. Therefore, the generation of the target state with $N_{\max} = 2$ needs 8 steps.

Our algorithm takes a quadratic number of steps while an exponential one is required in Ref. [20]. Let us now analyze the reason. Our algorithm employs four interaction Hamiltonians, $H_{\bar{1}0}$, $H_{0\bar{1}}$, H_{00} , and $H_{1\bar{1}}$, given in Eqs. (37), (34), (28), and (34), respectively. However, four interaction Hamiltonians “ $\hat{a}_x\sigma^+ + \text{H.c.}$ ”, “ $\hat{a}_y^\dagger\sigma^- + \text{H.c.}$ ”, “ $\sigma^- + \sigma^+$ ”, and “ $\hat{a}_x\hat{a}_y\sigma^+ + \text{H.c.}$ ” are employed in Ref. [20]. The former three interaction Hamiltonians between our algorithm and those in Ref. [20] are qualitatively identical since they convert the same number of bosons for either mode when the two-level system is excited. However, the last ones show fundamental difference between our algorithm and that in Ref. [20]. Because ours creates one boson (photon) of one mode but annihilate one boson (photon) of the other when the two-level system is excited, while in Ref. [20], one boson for each mode can be simultaneously created when the two-level system is excited. This difference is critical for us to design an algorithm which can keep track of the populations with a constant total boson (photon) number, i.e., $n_1 + n_2 = 0, 1, 2, \dots$, in sequence. Therefore, there is no leakage of the populations into the irrelevant space. However, the algorithm in Ref. [20] has population leakage. Obviously, if the last interaction in Ref. [20] is changed to “ $\hat{a}_x^\dagger\hat{a}_y\sigma^+ + \text{H.c.}$ ”, a theoretically equivalent algorithm to ours can also be developed. In this sense, our algorithm can be regarded as the improved version of that in Ref. [20].

B. Calculation of controllable parameters

Let us now study how to choose the pulse duration t_ν , the frequency $\tilde{\omega}_\nu$ and phase ϕ_ν of the driving field to generate a target state in the ν th step for different types of transitions.

(1) When we consider the transition “ $0\bar{1}$ ”, then $p_\nu = \bar{0}\bar{1}$ and the frequency of the driving field satisfies the condition $\tilde{\omega}_\nu = \omega_z - \omega_2$. Assuming we expect to transfer the population on the state $|n_1, n_2 + 1\rangle|g\rangle$ to the state $|n_1, n_2\rangle|e\rangle$, then we need to solve the following equation,

$$\bar{U}_\nu^\dagger(0) U_{\bar{1}}^{0\bar{1}\dagger}(t_\nu) \bar{U}_\nu(t_\nu) |\varphi_\nu\rangle = |\varphi_{\nu-1}\rangle, \quad (47)$$

where

$$|\varphi_\nu\rangle = c_\nu |n_1, n_2 + 1\rangle|g\rangle + d_\nu |n_1, n_2\rangle|e\rangle, \quad (48)$$

$$|\varphi_{\nu-1}\rangle = d_{\nu-1} |n_1, n_2\rangle|e\rangle. \quad (49)$$

are the projections on the Hilbert space spanned by $\{|n_1, n_2 + 1\rangle|g\rangle, |n_1, n_2\rangle|e\rangle\}$ of the state $|\psi_\nu\rangle$ for the ν th step and the state $|\psi_{\nu-1}\rangle$ for the $(\nu - 1)$ th step. Substituting Eqs. (45) and 35 into Eq. (47), we thus have the explicit solution for t_ν as

$$t_\nu = \frac{1}{|\Omega_{1n_1n_2}^{0\bar{1}}|} \arctan \left| \frac{c_\nu}{d_\nu} \right|, \quad (50)$$

and the phase of the driving field is determined by

$$0 = \frac{\pi}{2} - \arg \frac{d_\nu}{c_\nu} - x \sin(\tilde{\omega}_\nu t_\nu + \phi_\nu) - \tilde{\omega}_\nu t_\nu + \phi_{1n_1n_2}^{0\bar{1}\nu} \bmod 2\pi. \quad (51)$$

Here, the notation $\phi_{Nn_1n_2}^{k_1k_2\nu}$ is the value of $\phi_{Nn_1n_2}^{k_1k_2}$ for the ν th step, which is given in Eq. (32) and depends on ϕ_ν .

(2) When we consider the transition “ $\bar{1}0$ ”, then $p_\nu = \bar{1}0$ and the driving frequency should be tuned to $\tilde{\omega}_\nu = \omega_z - \omega_1$. Assuming we expect to transfer the population on the state $|n_1, n_2\rangle|e\rangle$ to the state $|n_1 + 1, n_2\rangle|g\rangle$, then from Eq. (46), we need to solve the following equation

$$\bar{U}_\nu^\dagger(0) U_{\bar{1}}^{\bar{1}0\dagger}(t_\nu) \bar{U}_\nu(t_\nu) |\varphi_\nu\rangle = |\varphi_{\nu-1}\rangle, \quad (52)$$

where

$$|\varphi_\nu\rangle = c_\nu |n_1 + 1, n_2\rangle|g\rangle + d_\nu |n_1, n_2\rangle|e\rangle, \quad (53)$$

$$|\varphi_{\nu-1}\rangle = c_{\nu-1} |n_1 + 1, n_2\rangle|g\rangle, \quad (54)$$

are the projections on the Hilbert space spanned by $\{|n_1 + 1, n_2\rangle|g\rangle, |n_1, n_2\rangle|e\rangle\}$ of the state $|\psi_\nu\rangle$ for ν th step and the state $|\psi_{\nu-1}\rangle$ for the $(\nu - 1)$ th step. Substituting Eqs. (45) and (38) into Eq. (52), we thus have the solution for t_ν

$$t_\nu = \frac{1}{|\Omega_{1n_1n_2}^{\bar{1}0}|} \arctan \left| \frac{d_\nu}{c_\nu} \right|, \quad (55)$$

and the phase of the driving field is determined by

$$0 = -\frac{\pi}{2} - \arg \frac{d_\nu}{c_\nu} - x \sin(\tilde{\omega}_\nu t_\nu + \phi_\nu) - \tilde{\omega}_\nu t_\nu + \phi_{1n_1n_2}^{\bar{1}0\nu} \bmod 2\pi. \quad (56)$$

Moreover, Assuming we expect to transfer the state $|n_1 + 1, n_2\rangle|g\rangle$ to the state $|n_1, n_2\rangle|e\rangle$, then Eq. (54) is changed into $|\varphi_{\nu-1}\rangle = d_{\nu-1} |n_1, n_2\rangle|e\rangle$. Similarly, we have the explicit solution for t_ν and the expression to determine ϕ_ν as below,

$$t_\nu = \frac{1}{|\Omega_{1n_1n_2}^{\bar{1}0}|} \arctan \left| \frac{c_\nu}{d_\nu} \right|, \quad (57)$$

$$0 = \frac{\pi}{2} - \arg \frac{d_\nu}{c_\nu} - x \sin(\tilde{\omega}_\nu t_\nu + \phi_\nu) - \tilde{\omega}_\nu t_\nu + \phi_{1n_1n_2}^{\bar{1}0\nu} \bmod 2\pi. \quad (58)$$

(3) When we consider the transition “ $1\bar{1}$ ”, then $p_\nu = 1\bar{1}$ and the frequency of the driving field should be tuned to

$$\tilde{\omega}_\nu = \omega_z + \omega_1 - \omega_2. \quad (59)$$

Assuming we expect to transfer the population on the state $|n_1, n_2 + 1\rangle|g\rangle$ to the state $|n_1 + 1, n_2\rangle|e\rangle$, then from Eq. (46), we need to solve the following equation,

$$\bar{U}_\nu^\dagger(0) U_{\bar{1}}^{1\bar{1}\dagger}(t_\nu) \bar{U}_\nu(t_\nu) |\varphi_\nu\rangle = |\varphi_{\nu-1}\rangle, \quad (60)$$

where

$$|\varphi_\nu\rangle = c_\nu |n_1, n_2 + 1\rangle|g\rangle + d_\nu |n_1 + 1, n_2\rangle|e\rangle, \quad (61)$$

$$|\varphi_{\nu-1}\rangle = d_{\nu-1} |n_1 + 1, n_2\rangle|e\rangle \quad (62)$$

are the projections on the Hilbert space spanned by $\{|n_1, n_2 + 1\rangle|g\rangle, |n_1 + 1, n_2\rangle|e\rangle\}$ of the state $|\psi_\nu\rangle$ for the ν th step and the state $|\psi_{\nu-1}\rangle$ for the $(\nu - 1)$ th step, respectively. Substituting Eqs. (45) and (35) into Eq. (60), we have the solution for t_ν as

$$t_\nu = \frac{1}{|\Omega_{1n_1n_2}^{1\bar{1}}|} \arctan \left| \frac{c_\nu}{d_\nu} \right|, \quad (63)$$

and the phase of the driving field is determined by the following equation

$$0 = \frac{\pi}{2} - \arg \frac{d_\nu}{c_\nu} - x \sin(\tilde{\omega}_\nu t_\nu + \phi_\nu) - \tilde{\omega}_\nu t_\nu + \phi_{1n_1n_2}^{1\bar{1}\nu} \bmod 2\pi. \quad (64)$$

(4) When we consider the transition “ 00 ”, then $p_\nu = 00$ and the frequency of the driving field should satisfy the condition $\tilde{\omega}_\nu = \omega_z$. Assuming we expect to transfer the population on the state $|n_1, n_2\rangle|e\rangle$ to the state $|n_1, n_2\rangle|g\rangle$, then we need to solve the following equation,

$$\bar{U}_\nu^\dagger(0) U_{\bar{1}}^{00\dagger}(t_\nu) \bar{U}_\nu(t_\nu) |\varphi_\nu\rangle = |\varphi_{\nu-1}\rangle \quad (65)$$

where

$$|\varphi_\nu\rangle = c_\nu |n_1, n_2\rangle|g\rangle + d_\nu |n_1, n_2\rangle|e\rangle, \quad (66)$$

$$|\varphi_{\nu-1}\rangle = c_{\nu-1} |n_1, n_2\rangle|g\rangle. \quad (67)$$

are the projections on the Hilbert space spanned by $\{|n_1, n_2\rangle|g\rangle, |n_1, n_2\rangle|e\rangle\}$ of the state $|\psi_\nu\rangle$ for the ν th step and the state $|\psi_{\nu-1}\rangle$ for the $(\nu - 1)$ th step, respectively. Substituting Eqs. (45) and (29) into Eq. (65), we have the solution

$$t_\nu = \frac{1}{|\Omega_{1n_1n_2}^{00}|} \arctan \left| \frac{d_\nu}{c_\nu} \right|, \quad (68)$$

and the phase of the driving field is determined by

$$0 = -\frac{\pi}{2} - \arg \frac{d_\nu}{c_\nu} - x \sin(\tilde{\omega}_\nu t_\nu + \phi_\nu) - \tilde{\omega}_\nu t_\nu + \phi_{1n_1n_2}^{00\nu} \bmod 2\pi. \quad (69)$$

According to the target state, the time duration, frequency and phase of the driving field for each step can be calculated using above equations. For example, if the “ 00 ” transition is used in the 3rd step, then we use Eq. (68) and Eq. (69) to obtain t_3 and ϕ_3 by setting $\nu = 3$.

C. Application to NOON states

As an example, we now apply our algorithm to the generation of the NOON state, i.e., the target state is

$$|\psi_f\rangle = \frac{1}{\sqrt{2}} (|N_{\max}, 0\rangle|g\rangle + |0, N_{\max}\rangle|g\rangle). \quad (70)$$

The recursion algorithm restoring $|\psi_f\rangle$ to the vacuum state $|0, 0\rangle|g\rangle$ is schematically shown in Fig. 3 for the maximum photon number $N_{\max} = 2$. In Fig. 3(a), we can find that all the populations in the Hilbert space spanned by $\{|0, 2\rangle|g\rangle, |2, 0\rangle|g\rangle\}$ can be transferred to the state $|1, 0\rangle|e\rangle$ by consecutively using transitions “0̄1”, “̄10”, “01”, and “̄10”. After this step, as schematically shown in Fig. 3(b), all the populations on the state $|1, 0\rangle|e\rangle$ can be transferred to the state $|0, 0\rangle|g\rangle$ by consecutively using transitions “00”, “̄10”, and “00”. The total step number is $f = 7$ for generating the NOON state $(|0, 2\rangle + |2, 0\rangle)/\sqrt{2}$.

More generally, given an arbitrary N_{\max} , the total step number for generating the NOON state in Eq. (70) is

$$f = 4N_{\max} - 1. \quad (71)$$

The step number for generating NOON state has been greatly reduced in comparing with that for generating an arbitrary state in Eq. (A18). Obviously, the NOON state can be generated without using the “1̄1” transition. If we assume the Lamb-Dicke parameter $\eta_l \lesssim 1$, which is usually the case even in the ultrastrong regime in superconducting circuit QED systems [36–38]. From Eq. (22), we have the Rabi frequencies $|\Omega_{In_1n_2}^{00}| \propto \eta_1^0\eta_2^0$, $|\Omega_{In_1n_2}^{11}| \propto \eta_1\eta_2$, $|\Omega_{In_1n_2}^{10}| \propto \eta_1$, and $|\Omega_{In_1n_2}^{01}| \propto \eta_2$. Thus, the transition “1̄1” generally takes more time among the four types of transitions employed by us. Therefore, our algorithm may show a better efficiency for generating NOON states than generating arbitrary entangled states. This is especially true when the maximal photon number N_{\max} is higher and the Lamb-Dicke parameter η_l is smaller.

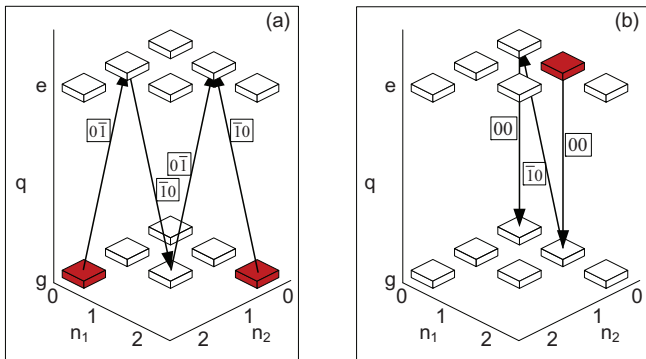


FIG. 3: (Color online) Application of the general algorithm to generating the NOON state. The notations are the same as those in Fig. 2. (a) Schematic diagram for transferring the population in the space $\{|0, 2\rangle|g\rangle, |2, 0\rangle|g\rangle\}$ to the state $|1, 0\rangle|e\rangle$. This is achieved by consecutively using “0̄1”, “̄10”, “01”, and “̄10” transitions. (b) Schematic diagram for transferring the population on the state $|1, 0\rangle|e\rangle$ to the state $|0, 0\rangle|g\rangle$. This is achieved by consecutively using “00”, “̄10”, and “00” transitions.

IV. MINIMIZING THE EFFECT OF UNWANTED TERMS

A. Theoretical analysis

In all of the above studies, we make an approximation that all unwanted terms have been neglected. However, these neglected nonresonant terms will affect the fidelity of the prepared target state. Let us now discuss how to minimize the effect of these unwanted terms in Eq. (20) on the target state by choosing appropriate parameters. In principle, the effects of these unwanted terms can be perfectly removed by pulse calibration techniques. Here, we study a method to minimize the effect of these unwanted terms by choosing the parameters when the pulse calibration cannot be used.

In our algorithm, we have used four interactions $H_{\bar{1}}^{10}$, $H_{\bar{1}}^{01}$, $H_{\bar{1}}^{1\bar{1}}$, and $H_{\bar{1}}^{00}$, all of them are constructed by the terms with the Bessel function $J_{\bar{1}}(x)$ in Eq. (20). Here, the representation of Bessel functions also uses \bar{k} to denote $-k$ when $k > 0$. We hope to suppress all the terms with the Bessel functions $J_N(x)$ for $N \neq -1$. We focus on the case $x = 2\Omega/\tilde{\omega} \sim 1$ considering possible experimental conditions. In this case, only lower order Bessel functions $J_0(x)$, $J_{\pm 1}(x)$, and $J_{\pm 2}(x)$ play significant roles. Thus, we need only to find proper parameters such that the effect of the terms with $J_0(x)$, $J_1(x)$, and $J_{\pm 2}(x)$ are negligibly small. Our idea is to make those terms nonresonant by properly choosing the parameters ω_x and ω_z of the qubit, and frequencies ω_1 and ω_2 of two microwave modes. That is, we assume that the frequency of the l th cavity mode satisfies

$$\omega_l = l_l \omega_{\text{gcd}}, \quad (72)$$

where l_l is a positive integer and ω_{gcd} is the greatest common divisor of ω_1 and ω_2 . Assuming that the “ $k_1 k_2$ ” transition is switched on, i.e., the transition detuning $\Delta_1^{k_1 k_2} = 0$, then from Eq. (23), the frequency $\tilde{\omega}$ of the driving field must satisfy the condition

$$\tilde{\omega} = \omega_z + k_1 \omega_1 + k_2 \omega_2. \quad (73)$$

From Eqs. (20), (72), and (73), the detuning of the terms with N, k'_1, k'_2 is then given by

$$\Delta_N^{k'_1 k'_2} = (N + 1) \omega_z + \sum_{l=1}^2 (N k_l + k'_l) l_l \omega_{\text{gcd}}. \quad (74)$$

Thus the terms with the Bessel function $J_1(x)$ will have the detuning

$$\Delta_1^{k'_1 k'_2} = 2\omega_z + \sum_{l=1}^2 (k_l + k'_l) l_l \omega_{\text{gcd}}. \quad (75)$$

We expect that the terms with $J_1(x)$ are nonresonant. Thus, the relation that $\Delta_1^{k'_1 k'_2} \neq 0$ must hold. A simple but sufficient condition is

$$2\omega_z \neq k \omega_{\text{gcd}}, \quad (76)$$

where k is an integer. Similarly, for the terms with $J_0(x)$, $J_2(x)$, and $J_{\bar{2}}(x)$, the sufficient conditions can be given by

$$\omega_z \neq k \omega_{\text{gcd}}, \quad (77)$$

$$3\omega_z \neq k \omega_{\text{gcd}}, \quad (78)$$

$$\omega_z \neq k \omega_{\text{gcd}}. \quad (79)$$

The conditions in Eqs. (76)-(79) can be summarized as

$$6\omega_z \neq k \omega_{\text{gcd}}. \quad (80)$$

We can also assume that the parameter ω_z of the qubit is

$$\omega_z = (p + r) \omega_{\text{gcd}}, \quad (81)$$

where p is the integer part, and r is the fraction part. To meet Eq. (80), there should be

$$r \notin \left\{ 0, \frac{1}{6}, \frac{2}{6}, \frac{3}{6}, \frac{4}{6}, \frac{5}{6} \right\}. \quad (82)$$

The nonresonant terms with J_1 , J_0 , and $J_{\pm 2}$ have effect on the desired time evolution. These effects can be further eliminated by decreasing the transition amplitudes $\Omega_{Nn_1n_2}^{k'_1k'_2}$ given in Eq. (22). The ideal case is

$$\left| \Omega_{Nn_1n_2}^{k'_1k'_2} \right| \ll |\Delta_N^{k'_1k'_2}|, \quad (83)$$

for $N = 0, 1, \pm 2$, and $n_1 + n_2 \leq N_{\text{max}}$, where the constraint condition for n_1 and n_2 denotes the working space of our algorithm. Considering that N_{max} is the maximum photon number of the target state, and using Eq. (74) and Eq. (81), we can obtain

$$\left| \Delta_0^{k'_1k'_2} \right| \geq r\omega_{\text{gcd}} \text{ or } (1-r)\omega_{\text{gcd}} \quad (84)$$

$$\left| \Delta_1^{k'_1k'_2} \right| \geq (2r - \lfloor 2r \rfloor) \omega_{\text{gcd}} \text{ or } (\lceil 2r \rceil - 2r) \omega_{\text{gcd}}, \quad (85)$$

$$\left| \Delta_2^{k'_1k'_2} \right| \geq (3r - \lfloor 3r \rfloor) \omega_{\text{gcd}} \text{ or } (\lceil 3r \rceil - 3r) \omega_{\text{gcd}}, \quad (86)$$

$$\left| \Delta_{\bar{2}}^{k'_1k'_2} \right| \geq r\omega_{\text{gcd}} \text{ or } (1-r)\omega_{\text{gcd}}. \quad (87)$$

Here, $\lfloor x \rfloor$ means x rounded down and $\lceil x \rceil$ means x rounded up. We thus reduce Eq. (83) to

$$\left| \Omega_{0n_1n_2}^{k'_1k'_2} \right| \ll \min\{r, 1-r\}\omega_{\text{gcd}}, \quad (88)$$

$$\left| \Omega_{1n_1n_2}^{k'_1k'_2} \right| \ll \min\{2r - \lfloor 2r \rfloor, \lceil 2r \rceil - 2r\}\omega_{\text{gcd}}, \quad (89)$$

$$\left| \Omega_{2n_1n_2}^{k'_1k'_2} \right| \ll \min\{3r - \lfloor 3r \rfloor, \lceil 3r \rceil - 3r\}\omega_{\text{gcd}}, \quad (90)$$

$$\left| \Omega_{\bar{2}n_1n_2}^{k'_1k'_2} \right| \ll \min\{r, 1-r\}\omega_{\text{gcd}}, \quad (91)$$

a condition much stronger than Eq. (83). If Eqs. (88)-(91) are fulfilled, the nonresonant terms can be in principle suppressed. We know from Eq. (22) that Eqs. (88)-(91) can be satisfied if, for example, the parameter ω_x of the qubit is tuned sufficiently small, assuming that the reduced driving frequency x and Lamb-Dicke parameters η_l have been appropriately chosen.

There are also unwanted resonant terms with the Bessel function $J_{\bar{1}}(x)$, which, however, also satisfy the resonant condition

$$\Delta_{\bar{1}}^{k'_1k'_2} = \sum_{l=1}^2 (k'_l - k_l) l_l \omega_{\text{gcd}} = 0. \quad (92)$$

We have used Eq. (74) to obtain Eq. (92). The Lamb-Dicke parameters satisfy the condition $\eta_l = 2g_l/\omega_l \lesssim 1$ for circuit QED systems even in the ultrastrong regime [36–38]. From Eq. (72), we know that l_1 and l_2 are coprime numbers. We can further make l_1 (or l_2) sufficiently large. Thus the undesired resonant terms will possess large $|k'_1|$ (or $|k'_2|$). In this way, the effects of these terms will be suppressed due to the exponential decrease via the term $\eta_l^{|k_l|}$ in Eq. (22). The condition, that the term $J_{\bar{1}}(x)$ is negligibly small, can be summarized as that l_1 and l_2 should satisfy

$$\eta_1^{l_2} \eta_2^{l_1} \ll 1. \quad (93)$$

We now summarize the condition that minimizes the effects of unwanted terms. The parameter ω_z of the qubit should satisfy Eq. (81) and Eq. (82). However, the parameter ω_x of the qubit is mainly constrained by current experiments. For example, typical values of $\omega_x/2\pi$ are in the range $1 \sim 5$ GHz. The frequencies of the cavity modes ω_l should satisfy Eq. (72) and Eq. (93). The values of the reduced driving frequency $x = 2\Omega/\tilde{\omega}$ and Lamb-Dicke parameter $\eta_l = 2g_l/\omega_l$ should satisfy Eq. (83) or stronger conditions Eqs. (88)-(91). Appropriate values of x and η_l can be obtained via numerical simulations, which will be discussed below in Sec. IV B.

B. Numerical simulations

We now further numerically simulate the effect of the unwanted terms on the generation of target states by using examples of generating the following two target states

$$\left| \tilde{\psi}_E \right\rangle = \sum_{n_1+n_2 \leq 2} \frac{1}{\sqrt{6}} |n_1, n_2\rangle |g\rangle, \quad (94)$$

$$\left| \tilde{\psi}_N \right\rangle = \frac{1}{\sqrt{2}} (|0, 2\rangle + |2, 0\rangle) |g\rangle, \quad (95)$$

for some given parameters. It is obvious that $|\tilde{\psi}_E\rangle$ is an entangled state where every state component is evenly occupied. We thus call $|\tilde{\psi}_E\rangle$ the evenly-populated state. The state $|\tilde{\psi}_N\rangle$ is a two-photon NOON state [5]. Both $|\tilde{\psi}_E\rangle$ and $|\tilde{\psi}_N\rangle$ possess a maximum photon number $N_{\text{max}} = 2$. The fidelities for generating these two states $|\tilde{\psi}_E\rangle$ and $|\tilde{\psi}_N\rangle$ are defined as

$$\mathcal{F}_E = \left| \left\langle \tilde{\psi}_E^A \right| \tilde{\psi}_E \right\rangle, \quad (96)$$

$$\mathcal{F}_N = \left| \left\langle \tilde{\psi}_N^A \right| \tilde{\psi}_N \right\rangle. \quad (97)$$

Here, $|\tilde{\psi}_E^A\rangle$ and $|\tilde{\psi}_N^A\rangle$ are respectively the actually generated states via the total Hamiltonian in Eq. (6).

TABLE I: The fidelities $\mathcal{F}_E = |\langle \tilde{\psi}_E^A | \tilde{\psi}_E \rangle|$ of the target state $|\tilde{\psi}_E\rangle = \sum_{n_1+n_2 \leq 2} (1/\sqrt{6}) |n_2, n_2\rangle |g\rangle$ are listed for different values of the reduced driving frequency $x = 2\Omega/\tilde{\omega}$ and the Lamb-Dicke parameter $\eta = 2g_1/\omega_1 = 2g_2/\omega_2$. Here $|\tilde{\psi}_E^A\rangle$ is the actually generated state using the total Hamiltonian. We have chosen the longitudinal frequency of the qubit $\omega_z/2\pi = 19.5$ GHz, the transverse frequency of the qubit $\omega_x/2\pi = 1.2$ GHz, the frequency of the first mode $\omega_1/2\pi = 6$ GHz and the frequency of the second mode $\omega_2/2\pi = 8$ GHz.

		η					
		0.2	0.3714	0.4571	0.5429	0.6286	0.7143
x	0.3	0.115	0.393	0.519	0.608	0.739	0.675
	0.7857	0.589	0.817	0.872	0.851	0.911	0.852
	1.0286	0.615	0.85	0.876	0.906	0.886	0.857
	1.2714	0.724	0.872	0.886	0.906	0.852	0.878
	1.7571	0.821	0.939	0.899	0.859	0.825	0.837
	2	0.867	0.915	0.838	0.876	0.887	0.859

We now determine the detailed experimental parameters. From Eq. (81) and Eq. (82), we set $r = 3/4$, $p = 9$, and $\omega_{\text{gcd}}/2\pi = 2$ GHz, which corresponds to $\omega_z/2 = 19.5$ GHz. From Eq. (83) or Eqs. (88)-(91), the parameter $\omega_x/2\pi$ should be made smaller, e.g., we set $\omega_x/2\pi = 1.2$ GHz. The frequency of the l th cavity, i.e., ω_l , is determined by Eq. (72) and (93). Since the microwave fields are usually of several gigahertz, here we set $l_1 = 3$, and $l_2 = 4$, thus yielding $\omega_1/2\pi = l_1\omega_{\text{gcd}}/2\pi = 6$ GHz and $\omega_2/2\pi = l_2\omega_{\text{gcd}}/2\pi = 8$ GHz. The Lamb-Dicke parameters for the first and second cavity modes are set to be identical, i.e.,

$$\eta_1 = \eta_2 = \eta. \quad (98)$$

We vary the Lamb-Dicke parameter η and the reduced driving frequency $x = 2\Omega/\tilde{\omega}$ to simulate the effect of the unwanted terms on the fidelity of the expected target states in Eqs. (94) and (95). The simulation results for generating target states in Eq. (94) and Eq. (95) are listed in Table I and Table II, respectively. We can easily find that larger reduced driving strengths x and Lamb-Dicke parameters η can make the fidelity higher. For the evenly-populated state $|\psi_E\rangle$, the largest fidelity 0.939 can be obtained at $x = 1.7571$ and $\eta = 0.3714$. However, for the NOON state $|\tilde{\psi}_N\rangle$, the largest fidelity 0.92 can be obtained at $x = 2$ and $\eta = 0.5429$.

V. ENVIRONMENTAL EFFECT ON TARGET STATES

In the above, we only discuss the effect of unwanted terms on the generation of target states. We now study the effect of dissipation on the fidelities of target states by numerical simulation for given parameters. When the environmental effect is included, the dynamical evolution of the SQC can be described by the master equation

$$\begin{aligned} \rho = & -i[H, \rho] + \mathcal{D}[\sqrt{\gamma_{eg}}\tilde{\sigma}_{ge}]\rho + \mathcal{D}[\sqrt{\gamma_{ee}}\tilde{\sigma}_{ee}]\rho \\ & + \mathcal{D}[\sqrt{\gamma_{gg}}\tilde{\sigma}_{gg}]\rho + \mathcal{D}[\sqrt{\kappa_1}a_1]\rho + \mathcal{D}[\sqrt{\kappa_2}a_2]\rho, \end{aligned} \quad (99)$$

TABLE II: The fidelities $\mathcal{F}_N = |\langle \tilde{\psi}_N^A | \tilde{\psi}_N \rangle|$ of the target state $|\tilde{\psi}_{\text{NOON}}\rangle = (1/\sqrt{2})(|0, 2\rangle |g\rangle + |2, 0\rangle |g\rangle)$ are listed for different values of the reduced driving frequency $x = 2\Omega/\tilde{\omega}$ and the Lamb-Dicke parameter $\eta = 2g_1/\omega_1 = 2g_2/\omega_2$. Here $|\tilde{\psi}_N^A\rangle$ is the actually generated state using the total Hamiltonian. We have chosen the same parameters as in Table. I.

		η					
		0.2	0.3714	0.4571	0.5429	0.6286	0.7143
x	0.3	0.108	0.34	0.403	0.395	0.461	0.687
	0.7857	0.675	0.815	0.833	0.862	0.829	0.868
	1.0286	0.78	0.857	0.846	0.867	0.883	0.813
	1.5143	0.871	0.877	0.873	0.877	0.787	0.806
	1.7571	0.844	0.918	0.889	0.902	0.862	0.819
	2	0.876	0.909	0.832	0.92	0.853	0.806

where ρ and H are the reduced density operator and the Hamiltonian of the whole system, respectively. The total Hamiltonian has been given in Eq. (6). The compact notation $\mathcal{D}[c]\rho = (2c\rho c^\dagger - c^\dagger c\rho - \rho c^\dagger c)/2$ represents the Lindblad-type dissipation. We have noted that $\{|g\rangle, |e\rangle\}$ is the basis of σ_z , but the qubit dissipation is determined in the basis $\{|\tilde{g}\rangle, |\tilde{e}\rangle\}$ of the qubit eigenstates. The ground ($|\tilde{g}\rangle$) and excited ($|\tilde{e}\rangle$) states of the qubit are given by the eigenstates of Eq. (2). If we define

$$\sigma_{\nu\mu} = |\nu\rangle \langle \mu|, \quad (100)$$

with $\nu = g, e$ and $\mu = g, e$, and also define

$$\tilde{\sigma}_{\nu\mu} = |\tilde{\nu}\rangle \langle \tilde{\mu}|, \quad (101)$$

with $\tilde{\nu} = \tilde{g}, \tilde{e}$ and $\tilde{\mu} = \tilde{g}, \tilde{e}$. We can easily verify

$$\tilde{\sigma}_{\nu\mu} = R_y(\theta) \sigma_{\nu\mu} R_y^\dagger(\theta),$$

where $R_y(\theta) = \exp(-i\theta\sigma_y/2)$, and $\theta = \arctan(\omega_x/\omega_z)$. In Eq. (99), γ_{eg} is the pure-relaxation rate from the qubit excited state to the ground state. Besides, γ_{gg} and γ_{ee} are the pure-dephasing rates originating from disturbed qubit eigenstates. The decay rates of the first and the second cavity fields are denoted by κ_1 and κ_2 , respectively.

Using parameters in Sec. IV B and taking the reduced driving strength $x = 2\Omega/\tilde{\omega} = 1.7571$ and Lamb-Dicke parameter $\eta = 0.3714$ from Table I and Table II, we find that the highest fidelity $\mathcal{F}_E = 0.939$ and $\mathcal{F}_N = 0.918$ are reached for generating the evenly-populated state $|\tilde{\psi}_E\rangle$ in Eq. (94) and the NOON state $|\tilde{\psi}_N\rangle$ in Eq. (95), respectively.

We now assume that the decay rates in Eq. (99) are taken as $\gamma_{gg}/2\pi = 0$, $\gamma_{ee}/2\pi = 2$ MHz, and $\gamma_{eg}/2\pi = \kappa_1/2\pi = \kappa_2/2\pi = 1$ MHz. We assume that ρ_E^A and ρ_N^A are the actually generated states for the target states $|\tilde{\psi}_E\rangle$ and $|\tilde{\psi}_{\text{NOON}}\rangle$. Then the fidelities can be redefined as

$$\mathcal{F}'_E = \sqrt{\langle \tilde{\psi}_E | \rho_E^A | \tilde{\psi}_E \rangle}, \quad (102)$$

$$\mathcal{F}'_N = \sqrt{\langle \tilde{\psi}_N | \rho_N^A | \tilde{\psi}_N \rangle}. \quad (103)$$

We perform numerical simulations using the above parameters and obtain $\mathcal{F}'_E = 0.911$ and $\mathcal{F}'_{\text{NOON}} = 0.863$. The total time for generating $|\tilde{\psi}_E\rangle$ is $T_E = 8.9561$ ns and that for generating $|\tilde{\psi}_N\rangle$ is $T_N = 10.4451$ ns. Both T_E and T_N are too small to induce significant decoherence at the decay rates specified by us. Thus, the fidelity losses induced by dissipation are fairly small, which are $\mathcal{F}_E - \mathcal{F}'_E = 0.028$ for the evenly-populated state $|\tilde{\psi}_E\rangle$ and $\mathcal{F}_N - \mathcal{F}'_N = 0.055$ for the NOON state $|\tilde{\psi}_N\rangle$.

VI. DISCUSSIONS

We now discuss the difference between our algorithm and the previous ones for generating arbitrary states of two cavity fields or two vibrational modes via a single two-level system.

Ref. [20] provided an algorithm to generate arbitrary states of two vibrational modes. But due to population leakage into irrelevant states, it takes an exponential complexity of the number of steps. The succeeding proposals [21–27] overcome the exponential drawback in several ways. Refs. [21, 22] use a third energy level of the atom to shield irrelevant oscillations. But higher levels usually have larger decay rates, which can reduce the fidelities of the target states. Refs. [25–27] use boson-number-dependent Stark effects to realize independent operations of particular states. But in this way, the detunings of nonresonant terms are usually less by one order of the coupling strengths between the two-level system and resonator modes. This means that the Rabi frequencies are smaller, and the longer generation time is required. Refs. [22, 24] use multiphoton processes of high photon number to shield irrelevant oscillations or reduce the number of steps. But if the coupling strengths between the atom and cavity fields are not high enough, then the Rabi frequencies become small, especially for states with high photon numbers, which obviously indicates longer generation time.

Our method has following advantages: (1) It only uses the two energy levels of the qubit. Thus, the fidelities of the target states should be higher because there is no other auxiliary energy levels. (2) The detunings of the nonresonant terms are in the order of the resonator frequencies, usually higher than the coupling strength between the qubit and resonator modes. Thus the Rabi frequency can be made bigger than that using boson-number-dependent Stark effects. (3) When we use multiphoton processes, a low photon number is converted in each step, i.e., one photon for either mode at most. Thus the Rabi frequency can be bigger than that using multiphoton processes of higher photon number, even though the coupling strengths between the qubit and cavity modes are not very big. Of course, stronger couplings will further enhance the Rabi frequencies and hence reduce the generation time.

We now compare the differences between our algorithm and other ones for generating NOON states.

Ref. [39] uses mutliphoton processes to generate NOON states. In superconducting systems, this means a low generation efficiency if the Lamb-Dicke parameter is not sufficiently big. Ref. [40] uses synchronization technology to generate

NOON states, but the time duration for synchronization between two steps can be quite long and there exists inevitably information leakage. Ref. [42] and its experimental realization [43] use two phase qubits with three active energy levels to generate NOON states of two cavity modes. The experimental setup is complex and the high energy levels of qubits will reduce the decoherence time. Ref. [25] uses photon number-dependent Stark effects to achieve independent operations. Thus the Rabi frequency is smaller than the qubit-cavity coupling strengths. Ref. [44] requires that two qubits be initially prepared in a Bell state and finally get decoupled from the qubits and cavity fields. Ref. [45] uses one qubit but still needs one additional level to shield unwanted resonances. More recently, Ref. [46] uses one qubit of four levels which resonantly interacts with two resonators simultaneously to speed up the generation process of NOON states.

When applied to generating NOON states, our algorithm has new features besides the common advantages for generating arbitrary two-mode photon states, due to the particularity of NOON states: (1) Only carrier processes and one-photon processes are used. In this case, even though the coupling strengths between the qubit and cavity modes are small, the large Rabi frequencies can still be obtained. (2) The number of steps is reduced to linear dependence on the maximum photon number. These advantages indicate less generation time and thus guarantee a higher efficiency than preceding methods.

Now we discuss the experimental feasibility of our scheme. Table I and Table II show that without pulse calibration, higher fidelities can be achieved at bigger Lamb-Dicke parameters η and reduced driving frequencies x . These values are already in the ultrastrong regime. Ref. [36] has reported ultrastrong couplings between three resonator modes and a flux qubit, where the Lamb-Dicke parameter η can reach as high as 0.236. In the ultrastrong regime, Rabi frequencies can be made to approach the magnitude of ω_x , which usually ranges from 1 to 5 GHz. The decay rates of the qubit and cavity fields are usually in the magnitude of megahertz. Thus the dissipation has small effect on the fidelities of target states. For singe-mode microwave fields, Fock states with up to six photons [9] and Fock state superpositions [10] have been experimentally demonstrated using phase qubits. The NOON state up to 3 photons has also been experimentally reported [43]. We thus hope that our proposal is also experimentally feasible in the near future.

VII. CONCLUSIONS

In summary, we have proposed an approach to generate arbitrary superpositions of photon states of two microwave fields in two separated cavities. Our method mainly depends on the coexistence of transverse and longitudinal couplings between the qubit and cavity fields. Employing the longitudinal couplings, we derive a Hamiltonian which is similar to that of trapped ions interacting with two vibrational modes [33]. Using four simple interaction Hamiltonians derived from the longitudinal coupling, we design the algorithm. Our algorithm can be regarded as the improved version of that

in [20] when the transverse and longitudinal couplings coexist in circuit QED systems. But it has remedied the drawback that the number of steps exponentially depends on the maximal photon number, which is replaced by a quadratic dependence. Compared with previous ones with quadratic complexity, our algorithm does not require atomic energy levels higher than two [21, 22], boson-number-dependent stark effects [23, 25, 27], or multiboson processes of high photon numbers [22, 24].

When applied to the generation of NOON states, whose engineering has been extensively studied [39–47], our algorithm needs no two-mode sideband transitions. Meanwhile, the number of steps only linearly depends on the maximum photon numbers. In fact, these properties for generating NOON states can be generalized to any states with a constant total photon number of both modes.

We have also discussed how to avoid the effect of unwanted terms on the generation of target state. Our numerical results show that fidelities above 0.91 can be reached in the ultra-strong regime for the two-photon evenly-populated state and NOON state when the environmental effect is neglected. The generation time can be very short, in which case, the environment has small effect on fidelities of the target states. We here note that due to the similarity of two-mode interaction Hamiltonians, the algorithm using two-mode multi-phonon processes in Ref. [24] can be directly applied into our model. Thus, two-mode Fock states with high photon numbers can be generated with just two steps as one-mode Fock states in [30].

We have noted that our method for generating NOON states is similar to a recent algorithm simplified from the one which employs Stark effects to generate arbitrary entangled states [27].

VIII. ACKNOWLEDGEMENT

YXL is supported by the National Basic Research Program of China Grant No. 2014CB921401, the NSFC Grants No. 61025022, and No. 91321208.

Appendix A: Universal algorithm for arbitrary maximum photon numbers

The basic principle of our algorithm is state space reduction. The state space of the target state in Eq. (42) can be denoted as

$$\mathcal{H}_{2N_{\max}} = \{|n_1, n_2\rangle |g\rangle |n_1 + n_2 \leq N_{\max}\}. \quad (\text{A1})$$

We will implement $2N_{\max}$ procedures, with each procedure containing some steps.

In the 1st procedure, we aim to clear the populations in the subspace

$$\mathcal{H}'_{2N_{\max}} = \{|n_1, n_2\rangle |g\rangle |n_1 + n_2 = N_{\max}\} \quad (\text{A2})$$

of $\mathcal{H}_{2N_{\max}}$. This can be achieved via alternatively switching N_{\max} "10" transitions and N_{\max} "01" transitions to transfer

the populations in the subspace $\mathcal{H}'_{2N_{\max}}$ of $\mathcal{H}_{2N_{\max}}$ to the state $|N_{\max} - 1, 0\rangle |e\rangle$. Thus, $\mathcal{H}_{2N_{\max}}$ is reduced to the state space $\mathcal{H}_{2N_{\max}-1}$ where

$$\begin{aligned} \mathcal{H}_{2N_{\max}-1} = & \{|n_1, n_2\rangle |g\rangle |n_1 + n_2 \leq N_{\max} - 1\} \\ & \cup \{|n_1, n_2\rangle |e\rangle |n_1 + n_2 \leq N_{\max} - 2\} \\ & \cup \{|N_{\max} - 1, 0\rangle |e\rangle\}. \end{aligned} \quad (\text{A3})$$

In the 2nd procedure, we aim to clear the populations in the subspace $\{|N_{\max} - 1, 0\rangle |e\rangle\}$ of $\mathcal{H}_{2N_{\max}-1}$. This can be achieved via alternatively switching $N_{\max} - 1$ "11" transitions and $N_{\max} - 1$ "00" transitions to transfer the populations in the subspace

$$\begin{aligned} \mathcal{H}'_{2N_{\max}-1} = & \{|n_1, n_2\rangle |g\rangle |n_1 + n_2 = N_{\max} - 1, n_2 \neq 0\} \\ & \cup \{|N_{\max} - 1, 0\rangle |e\rangle\} \end{aligned} \quad (\text{A4})$$

of $\mathcal{H}_{2N_{\max}-1}$ to the state $|N_{\max} - 1, 0\rangle |g\rangle$. Thus, $\mathcal{H}_{2N_{\max}-1}$ is reduced to the state space $\mathcal{H}_{2N_{\max}-2}$ where

$$\begin{aligned} \mathcal{H}_{2N_{\max}-2} = & \{|n_1, n_2\rangle |g\rangle |n_1 + n_2 \leq N_{\max} - 2\} \\ & \cup \{|n_1, n_2\rangle |e\rangle |n_1 + n_2 \leq N_{\max} - 2\} \\ & \cup \{|N_{\max} - 1, 0\rangle |g\rangle\}. \end{aligned} \quad (\text{A5})$$

In the 3rd procedure, we aim to clear the population in the subspace $\{|N_{\max} - 1, 0\rangle |g\rangle\}$ of $\mathcal{H}_{2N_{\max}-2}$. This can be achieved via alternatively switching $N_{\max} - 1$ "10" transitions and $N_{\max} - 2$ "01" transitions to transfer the populations in the subspace

$$\begin{aligned} \mathcal{H}'_{2N_{\max}-2} = & \{|n_1, n_2\rangle |e\rangle |n_1 + n_2 = N_{\max} - 2, n_2 \neq 0\} \\ & \cup \{|N_{\max} - 1, 0\rangle |g\rangle\} \end{aligned} \quad (\text{A6})$$

of $\mathcal{H}_{2N_{\max}-2}$ to the state $|N_{\max} - 2, 0\rangle |e\rangle$. Thus, $\mathcal{H}_{2N_{\max}-2}$ is reduced to the state space $\mathcal{H}_{2N_{\max}-3}$ where

$$\begin{aligned} \mathcal{H}_{2N_{\max}-3} = & \{|n_1, n_2\rangle |g\rangle |n_1 + n_2 \leq N_{\max} - 2\} \\ & \cup \{|n_1, n_2\rangle |e\rangle |n_1 + n_2 \leq N_{\max} - 3\} \\ & \cup \{|N_{\max} - 2, 0\rangle |e\rangle\}. \end{aligned} \quad (\text{A7})$$

⋮

In the 2μ th procedure, we aim to clear the population in the subspace $\{|N_{\max} - \mu, 0\rangle |e\rangle\}$ of $\mathcal{H}_{2N_{\max}-2\mu+1}$. This can be achieved via alternatively switching $N_{\max} - \mu$ "11" transitions and $N_{\max} - \mu$ "00" transitions to transfer the populations in the subspace

$$\begin{aligned} \mathcal{H}'_{2N_{\max}-2\mu+1} = & \{|n_1, n_2\rangle |g\rangle |n_1 + n_2 = N_{\max} - \mu, n_2 \neq 0\} \\ & \cup \{|N_{\max} - \mu, 0\rangle |e\rangle\} \end{aligned} \quad (\text{A8})$$

of $\mathcal{H}_{2N_{\max}-2\mu+1}$ to the state $|N_{\max} - \mu, 0\rangle |g\rangle$. Thus, $\mathcal{H}_{2N_{\max}-2\mu+1}$ is reduced to the state space $\mathcal{H}_{2N_{\max}-2\mu}$ where

$$\begin{aligned} \mathcal{H}_{2N_{\max}-2\mu} = & \{|n_1, n_2\rangle |g\rangle |n_1 + n_2 \leq N_{\max} - \mu - 1\} \\ & \cup \{|n_1, n_2\rangle |e\rangle |n_1 + n_2 \leq N_{\max} - \mu - 1\} \\ & \cup \{|N_{\max} - \mu, 0\rangle |g\rangle\}. \end{aligned} \quad (\text{A9})$$

In the $(2\mu + 1)$ th procedure, we aim to clear the population in the subspace $\{|N_{\max} - \mu, 0\rangle |g\rangle\}$ of $\mathcal{H}_{2N_{\max}-2\mu}$. This can be achieved via alternatively switching $N_{\max} - \mu$ "10" transitions and $N_{\max} - \mu - 1$ "01" transitions to transfer the populations in the subspace

$$\begin{aligned} \mathcal{H}'_{2N_{\max}-2\mu} = & \{|n_1, n_2\rangle |e\rangle |n_1 + n_2 = N_{\max} - \mu - 1, n_2 \neq 0\} \\ & \cup \{|N_{\max} - \mu, 0\rangle |g\rangle\} \end{aligned} \quad (\text{A10})$$

of $\mathcal{H}_{2N_{\max}-2\mu}$ to the state $|N_{\max} - \mu - 1, 0\rangle |e\rangle$. Thus, $\mathcal{H}_{2N_{\max}-2\mu}$ is reduced to the state space $\mathcal{H}_{2N_{\max}-2\mu-1}$ where

$$\begin{aligned} \mathcal{H}_{2N_{\max}-2\mu-1} = & \{|n_1, n_2\rangle |g\rangle |n_1 + n_2 \leq N_{\max} - \mu - 1\} \\ & \cup \{|n_1, n_2\rangle |e\rangle |n_1 + n_2 \leq N_{\max} - \mu - 2\} \\ & \cup \{|N_{\max} - \mu - 1, 0\rangle |e\rangle\}. \\ & \vdots \end{aligned} \quad (\text{A11})$$

In the $(2N_{\max} - 1)$ th procedure, we aim to clear the population in the subspace

$$\mathcal{H}'_2 = \{|1, 0\rangle |g\rangle\} \quad (\text{A12})$$

of \mathcal{H}_2 . This can be achieved via alternatively switching one "10" transition to transfer the populations in the subspace \mathcal{H}'_2 of \mathcal{H}_2 to the state $|0, 0\rangle |e\rangle$. Thus, \mathcal{H}_2 is reduced to the state space \mathcal{H}_1 where

$$\mathcal{H}_1 = \{|0, 0\rangle |q = g, e\rangle\}. \quad (\text{A13})$$

In the $2N_{\max}$ th procedure, we aim to clear the population in the subspace

$$\mathcal{H}'_1 = \{|0, 0\rangle |e\rangle\} \quad (\text{A14})$$

of \mathcal{H}_1 . This can be achieved via switching one "00" transitions to transfer the populations in the subspace \mathcal{H}'_1 of \mathcal{H}_1 to the state $|0, 0\rangle |g\rangle$. Thus, \mathcal{H}_1 is reduced to the state space \mathcal{H}_0 where

$$\mathcal{H}_0 = \{|0, 0\rangle |g\rangle\}, \quad (\text{A15})$$

is namely the initial state space for $|\psi_0\rangle$ in Eq. (43).

Based on the above discussion, we now calculate the number of steps to generate the target state in Eq. (42) with an arbitrary maximum photon number N_{\max} . For alternatively switching "11" and "00" transitions, we need $f_{11,00}$ steps, given by

$$f_{11,00} = 1 + \sum_{N=1}^{N_{\max}-1} 2N = N_{\max}^2 - N_{\max} + 1. \quad (\text{A16})$$

For alternatively switching "10" and "01" transitions, we need $f_{10,01}$ steps, given by

$$f_{10,01} = 1 + \sum_{N=1}^{N_{\max}} (2N - 1) = N_{\max}^2 + 1. \quad (\text{A17})$$

Therefore, the total step number f is

$$f = f_{11,00} + f_{10,01} = 2N_{\max}^2 - N_{\max} + 2. \quad (\text{A18})$$

for generating the target state as shown in Eq. (42).

[1] A. Blais, R. S. Huang, A. Wallraff, S. Girvin, and R. J. Schoelkopf, Phys. Rev. A **69**, 062320 (2004).
[2] A. Wallraff, D. I. Schuster, A. Blais, L. Frunzio, R. S. Huang, J. Majer, S. Kumar, S. M. Girvin, and R. J. Schoelkopf, Nature (London) **431**, 162 (2004).
[3] S. Ritter, C. Nölleke, C. Hahn, A. Reiserer, A. Neuzner, M. Uphoff, M. Mücke, E. Figueroa, J. Bochmann, and G. Rempe, Nature (London) **484**, 195 (2012).
[4] H. J. Kimble, Nature (London) **453**, 1023 (2008).
[5] M. A. Nielsen and I. L. Chuang, *Quantum Computation and Quantum Information* (Cambridge university press, 2010).
[6] M. O. Scully and M. S. Zubairy, *Quantum Optics* (Cambridge university press, 1997).
[7] Y. X. Liu, L. F. Wei, and F. Nori, Europhys. Lett. **67**, 941 (2014).
[8] Yu-xi Liu, L. F. Wei, and F. Nori, Phys. Rev. A **71**, 063820 (2005).
[9] M. Hofheinz, E. M. Weig, M. Ansmann, R. C. Bialczak, E. Lucero, M. Neeley, H. Wang, J. M. Martinis, and A. N. Cleland, Nature (London) **454**, 310 (2008).
[10] M. Hofheinz, H. Wang, M. Ansmann, R. C. Bialczak, E. Lucero, M. Neeley, A. D. O'Connell, D. Sank, J. Wenner, J. M. Martinis, and A. N. Cleland, Nature (London) **459**, 546 (2009).
[11] K. Vogel, V. Akulin, and W. Schleich, Phys. Rev. Lett. **71**, 1816 (1993).
[12] Y. Makhlin, G. Schön, and A. Shnirman, Rev. Mod. Phys. **73**, 357 (2001).
[13] J. Q. You and F. Nori, Phys. Today **58**, 42 (2005).
[14] G. Wendin and V. S. Shumeiko, Low Temp. Phys. **33**, 724 (2007).
[15] R. Schoelkopf and S. Girvin, Nature (London) **451**, 664 (2008).
[16] J. Clarke and F. K. Wilhelm, Nature (London) **453**, 1031 (2008).
[17] J. Q. You and F. Nori, Nature (London) **474**, 589 (2011).
[18] I. Buluta, S. Ashhab, and F. Nori, Rep. Prog. Phys. **74**, 104401 (2011).
[19] Z. L. Xiang, S. Ashhab, J. Q. You, and F. Nori, Rev. Mod. Phys. **85**, 623 (2013).
[20] S. A. Gardiner, J. I. Cirac, and P. Zoller, Phys. Rev. A **55**, 1683 (1997).
[21] G. Drobny, B. Hladký, and V. Bužek, Phys. Rev. A **58**, 2481 (1998).
[22] S. B. Zheng, Phys. Rev. A **63**, 015801 (2000).
[23] B. Kneer and C. K. Law, Phys. Rev. A **57**, 2096 (1998).

- [24] X. Zou, K. Pahlke, and W. Mathis, Phys. Rev. A **65**, 045801 (2002).
- [25] F. W. Strauch, K. Jacobs, and R. W. Simmonds, Phys. Rev. Lett. **105**, 050501 (2010).
- [26] F. W. Strauch, D. Onyango, K. Jacobs, and R. W. Simmonds, Phys. Rev. A **85**, 022335 (2012).
- [27] R. Sharma and F. W. Strauch, arXiv: 1503.02157 (2015).
- [28] Y. X. Liu, J. Q. You, L. F. Wei, C. P. Sun, and F. Nori, Phys. Rev. Lett. **95**, 087001 (2005).
- [29] Y. X. Liu, C. X. Yang, H. C. Sun, and X. B. Wang, New J. Phys. **16**, 015031 (2014).
- [30] Y. J. Zhao, Y. L. Liu, Y. X. Liu, and F. Nori, Phys. Rev. A **91**, 053820 (2015).
- [31] M. Sasura and V. Buzek, J. Mod. Opt. **49**, 1593 (2002).
- [32] L. F. Wei, Y. X. Liu, and F. Nori, Phys. Rev. A **70**, 063801 (2004).
- [33] J. Steinbach, J. Twamley, and P. Knight, Phys. Rev. A **56**, 4815 (1997).
- [34] J. M. Martinis, S. Nam, J. Aumentado, and C. Urbina, Phys. Rev. Lett. **89**, 117901 (2002).
- [35] J. Lisenfeld, A. Lukashenko, M. Ansmann, J. M. Martinis, and A. V. Ustinov, Phys. Rev. Lett. **99**, 170504 (2007).
- [36] T. Niemczyk, F. Deppe, H. Huebl, E. Menzel, F. Hocke, M. Schwarz, J. Garcia-Ripoll, D. Zueco, T. Hümmer, and E. Solano, Nat. Phys. **6**, 772 (2010).
- [37] P. Forn-Díaz, J. Lisenfeld, D. Marcos, J. J. García-Ripoll, E. Solano, C. J. P. M. Harmans, and J. E. Mooij, Phys. Rev. Lett. **105**, 237001 (2010).
- [38] R. Stassi, A. Ridolfo, O. Di Stefano, M. J. Hartmann, and S. Savasta, Phys. Rev. Lett. **110**, 243601 (2013).
- [39] X. B. Zou, J. Kim, and H. W. Lee, Phys. Rev. A **63**, 065801 (2001).
- [40] X. W. Xu, Y. J. Zhao, and Y. X. Liu, Phys. Rev. A **88**, 022325 (2013).
- [41] C. P. Yang, S. I. Chu, and S. Han, Phys. Rev. A **67**, 042311 (2003).
- [42] S. T. Merkel and F. K. Wilhelm, New J. Phys. **12**, 093036 (2010).
- [43] H. Wang, M. Mariantoni, R. C. Bialczak, M. Lenander, E. Lucero, M. Neeley, A. O'Connell, D. Sank, M. Weides, and J. Wenner, Phys. Rev. Lett. **106**, 060401 (2011).
- [44] F. W. Strauch, Phys. Rev. Lett. **109**, 210501 (2012).
- [45] Q. P. Su, C. P. Yang, and S. B. Zheng, Sci. Rep. **4**, 3898 (2014).
- [46] S.-J. Xiong, Z. Sun, J.-M. Liu, T. Liu, and C.-P. Yang, Opt. Lett. **40**, 2221 (2015).
- [47] Z. H. Peng, Y.-X. Liu, Y. Nakamura, and J. S. Tsai, Phys. Rev. B **85**, 024537 (2012).